Journal of Genetic Engineering and Biotechnology 23 (2025) 100539

Contents lists available at ScienceDirect

Journal of Genetic Engineering and Biotechnology

journal homepage: www.elsevier.com/locate/jgeb

Green synthesis of silver nanoparticles using *Pyrostegia venusta* extract, characterization and estimation of antioxidant, antiglycation and anti-aging activities

Regildo Márcio Gonçalves da Silva [a,b,*], Pedro Augusto Pereira Rosatto [a,c], Isabelly do Nascimento Pereira [a], Laura Camargo Zibordi [a], Hugo Henrique Santos [a], Filipe Oliveira Granero [b], Célia Cristina Malaguti Figueiredo [a,b], Patrícia Soares Santiago [c], Carlos Augusto Prata Gaona [c], Nilson Nicolau-Junior [d], Luciana Pereira Silva [b,e]

[a] São Paulo State University (UNESP), School of Sciences, Humanities and Languages, Department of Biotechnology, Laboratory of Herbal Medicine and Natural Products, Assis, São Paulo, Brazil
[b] São Paulo State University (UNESP), Institute of Chemistry, Araraquara, São Paulo, Brazil
[c] São Paulo State University (UNESP), School of Agricultural Sciences, Registro, São Paulo, Brazil
[d] Federal University of Uberlândia (UFU), Institute of Biotechnology, Laboratory of Molecular Modeling, Uberlândia, Minas Gerais, Brazil
[e] Fundação Educacional do Município de Assis (FEMA), Assis, São Paulo, Brazil

ARTICLE INFO

Keywords:
Aging
Enzyme inhibition
Flavonoids
Free radicals
Metallic nanoparticles
Protein glycation

ABSTRACT

Pyrostegia venusta presents phytoconstituents with biological properties including antioxidant activity. This study aimed to prepare *P. venusta* aqueous extract (PvAE), synthesize silver nanoparticles (AgNPs) through green synthesis using PvAE, determine their phytoconstituents, evaluate their in vitro antioxidants, antiglycation, and anti-aging activities, and analyze in silico docking of the main phenolic compounds. Phytoconstituents were identified by HPLC and determined by total polyphenols and flavonoids. AgNPs were characterized by scanning transmission electron microscopy and dynamic light scattering. Evaluation of antioxidant potential was performed by DPPH radical scavenging, FRAP, TBARS, ORAC, and oxidative hemolysis analysis. Evaluation of antiglycation activity was carried out by the determination of free amino groups, inhibition of AGEs formation, and REM assays. Anti-aging pandal was evaluated by in vitro and in silico assays. PvAE exhibited the highest total polyphenols (325.78 mg gallic acid equivalent g^{-1}), while AgNPs showed the highest total flavonoids (373.53 mg rutin equivalent g^{-1}). PvAE presented the highest antioxidant activity in DPPH test (74.90 %), although AgNPs exhibited antioxidant activity in ORAC, FRAP (862 μM Trolox equivalent g^{-1}), TBARS (53.97 % inhibition of TBARS formation), and oxidative hemolysis inhibition (85.36 %) assays. Antiglycation evaluation demonstrated the activity of PvAE and AgNPs. PvAE presented in vitro enzymes inhibition and in silico studies demonstrated possible active binding sites between P. venusta main compounds and enzymes that may be correlated with their potential to act at pre- and post-transcriptional levels. Therefore, this study provides information regarding P. venusta and demonstrates that further studies are needed to evaluate its application.

1. Introduction

Pyrostegia venusta (Ker Gawl.) Miers (family, Bignoniaceae) is a liana creeper known as "cipó-de-São-João" and it is considered of ecological and medicinal importance.[1] This species is commonly found in South and Southeast of Brazil, and it is ecologically characterized as an invasive plant that occurs on the edges of forests and roads. *P. venusta* exhibits intense flowering between June and August, and thus it is considered an ornamental winter species in Brazil.[2,3] In traditional medicine, *P. venusta* flower extracts are mainly employed for the treatment of vitiligo, although they are also used to treat intestinal and respiratory infections[4–6]. Scientific studies have reported antioxidant,

* Corresponding author at: São Paulo State University (UNESP), School of Sciences, Humanities and Languages, Department of Biotechnology, Laboratory of Herbal Medicine and Natural Products, Dom Antonio Avenue 2100, 19806-900, Assis, São Paulo, Brazil.
E-mail address: regildo.silva@unesp.br (R.M.G. Silva).

https://doi.org/10.1016/j.jgeb.2025.100539
Received 17 June 2025; Received in revised form 7 July 2025; Accepted 9 July 2025
Available online 25 July 2025

antimicrobial and wound-healing activities of different plant extracts from this species.[7,8] Besides, *P. venusta* plant extracts have demonstrated their activity against vitiligo due to the stimulation of melanin.[6,9,10] These biological activities are associated with the phytochemical composition of *P. venusta* extracts, which includes flavonoids, steroids, terpenoids, alkaloids, tannins, saponins, triterpenes, carbohydrates (*meso*-inositol), nitrogenous compounds (allantoin), n-alkanes (N-Hentriacontane), choline chloride, fatty acids, acacetin-7-O-β-glucopyranoside, iridoid glucosides, bellericanin glycosides, naphthoquinones, allotannic acids, oleanolic acid, and β-sitosterol.[11–13] Plant extracts can be prepared using different plant parts and a variety of techniques. Certain formulations of plant-based extracts may increase efficiency and stability of phytoconstituents and reduce toxicity.[14] The capacity of these plant extracts to treat and prevent human and animal diseases depends on the preparation methods by which phytochemical compounds are extracted from plant materials.[15]

Bionanotechnology has emerged as integration between biotechnology and nanotechnology. Considering that, green synthesis of nanomaterials emerges as an eco-friendly alternative for various applications, while ensuring stability and efficiency of natural active compounds.[16,17] The method of green synthesis of metal nanoparticles (NPs) is performed by utilizing compounds from plant extracts as bioreducing agents to offer a simple, highly efficient, economically viable, sustainable, and nontoxic alternative to chemical and physical methods of NPs synthesis.[18–20] Different metals can be used to obtain NPs including silver (Ag), platinum (Pt), gold (Au), and cobalt (Co), which have been reported to exhibit possible applications in catalysis, nanodevices, and nanomedicine chemistry, due to their electromagnetic, chemical, and physical characteristics.[21] One of the most studied NPs are those synthesized using Ag and phytoconstituents of extracts from different plant parts (e.g. roots, stems, leaves, flowers), which are crucial for the silver nanoparticles (AgNPs) synthesis.[22] Plants contain hydroxyl, carboxyl, carbonyl, amino, and phenol groups of phenolic acids (hydroxycinnamic, ellagic acids, and benzoic), anthocyanins, and flavonoids (flavan-3-ols, flavanols) that are responsible for their capacity to reduce metal salts and ultimately form AgNPs.[23] These NPs have been widely used as ingredients in several commercial products, and they have been applied in pharmaceutical, textile, food, cosmetic, electronic and energy industries.[24] Besides, they have been reported as anti-inflammatory, antidiabetic, antiviral, antibacterial, and antifungal agents, and more recently studies have demonstrated their activity against damage caused by oxidative stress.[25,26]

Oxidative stress is a process promoted by a persistent imbalance between excessive production of oxidative compounds (mainly free radicals) and limited antioxidant defenses, leading to tissue, cells and biomolecules damage. These oxidative compounds are predominantly generated in mitochondria during electron transport chain.[27] On the other hand, antioxidant defenses are responsible for the inhibition and/or reduction of damage caused by oxidative compounds. In addition, oxidative stress may be increased due to protein glycation, which is a process of covalent bonding between protein amino groups and reducing sugars, generating advanced glycation end-products (AGEs). These products are involved in various signal transduction mechanisms through AGEs receptor (RAGE) that may lead to cell disorders and dysfunction, contributing to pro-inflammatory response and production of reactive free radicals that may promote an increase in oxidative stress.[28] Free radicals and AGEs are associated with both oxidative stress and protein glycation, which are responsible for the appearance and development of degenerative diseases, which are correlated with premature aging caused by molecular damage that lead to cell alteration and/or death.[29,30]

Considering the above, the present study aimed to obtain and characterize AgNPs synthesized through green synthesis using *P. venusta* flower aqueous extract (PvAE) as bioreductor agent. Besides, it aimed to determine phytochemical composition (polyphenols and flavonoids) and evaluate their *in vitro* antioxidant, antiglycation, and anti-aging activities. It also aimed to analyze in silico molecular docking of the main phenolic compounds of PvAE.

2. Materials and methods

2.1. Collection and identification of plant material

P. venusta flowers were collected between June and August 2022 in Assis, São Paulo, Brazil, at the coordinates 22°32′26″S − 50°22′31″N and 22°32′18″S − 50°22′47″N. One specimen was taxonomically identified and deposited at the Herbarium of the Instituto Florestal de Assis under the voucher number SPSF − 40207.

2.2. Preparation of PvAE

P. venusta flowers were separated, washed, and dried in an air-forced oven at 40 °C. Dried flowers were grounded into a fine powder using a porcelain mortar. Aqueous extract was prepared by dissolving the plant material in ultrapure water at a proportion of 1:10 (w/v) under constant stirring. The mixture was then sonicated for 5 min at 50 Hz, followed by heating in a water bath for 20 min at 60 °C. After cooling to room temperature, the solution was filtered using Whatman No. 1 filter paper to obtain PvAE.

2.3. Phytochemical analysis of PvAE using high performance liquid chromatography (HPLC)

The phytochemical composition of PvAE was analyzed using a HPLC apparatus (Accela High Speed LC from Thermo Scientific®) with a photodiode array detector (PDA). The analysis was carried out by employing ultrapure water with 0.1 % formic acid as solvent A and methanol with 0.1 % formic acid as solvent B. Phenomenex® Luna C18 column (250 mm × 4.6 mm × 5 μm) was used at a temperature of at 25 °C and flow rate of 0.8 mL min^{-1}. The injection volume was 20 μL and detection was performed at 254 nm. A linear gradient elusion from 25 % A to 100 % B was employed for 80 min, followed by 5 min re-equilibration with 25 % B. The identification of polyphenols, including flavonoids and phenolic acids, was conducted based on comparisons with data reported in current literature.

2.4. Green synthesis and characterization of silver nanoparticles (AgNPs)

2.4.1. Synthesis of AgNPs

AgNPs were synthesized using a method designed by Vankudoth et al.[31] utilizing silver nitrate ($AgNO_3$, Sigma-Aldrich, Brazil) and PvAE as bioreducing and stabilizing agent. A solution containing 10 mL $AgNO_3$ (1, 5, or 10 mM) diluted in ultrapure water and 10 mL PvAE (0.3, 3.0, or 30 mg mL^{-1}) were mixed. The reaction conditions were optimized by altering pH levels (6, 10, or 13) and temperature/time parameters (30 °C for 60 min or 50 °C for 30 min). AgNPs formation was confirmed by a color change in solution from colorless to dark brown.

2.4.2. Characterization of AgNPs

AgNPs were identified with a UV-vis spectrophotometer (Bel Photonics, Brazil) to obtain the extinction spectra of AgNPs within the range of 350–650 nm. Peaks observed between 400 and 450 nm were attributed to the surface plasmon resonance of spherical nanoparticles as reported by Adrianto et al.[17]. Additional characterizations were performed with a Zetasizer 90 (Malvern) for zeta potential analysis and dynamic light scattering (DLS) for the determination of size distribution. A morphological evaluation was conducted utilizing a scanning transmission electron microscopy (STEM, Hitachi 3800U), where colloidal solutions were dried onto FORMVAR-coated copper grids for imaging. The characterization of the functional groups of synthesized silver nanoparticles was performed using Fourier transform infrared spectroscopy (FTIR).[32] The analyses were conducted with a Bruker

spectrometer (Alpha II, Billerica, MA, USA), operating in the spectral range of 1000 to 4000 cm^{-1}.

2.5. Determination of phytochemical compounds in PvAE and AgNPs

The method described by Singleton and Rossi[33] was used to evaluate total polyphenols content in PvAE and AgNPs, using Folin-Ciocalteu as reagent and gallic acid as standard. Absorbance of PvAE (0.3 or 30 mg mL^{-1}) or AgNPs was read at 765 nm using a UV-vis spectrophotometer (Bel Photonics, Brazil) and results were defined as mg of gallic acid equivalent (GAE) per gram of dry weight (DW).

The methodology of Christ and Müller[34] was used to evaluate total flavonoids content using rutin as standard. Absorbance of PvAE (0.3 or 30 mg mL^{-1}) or AgNPs was read at 510 nm, and results were defined as mg rutin equivalent (RE) per g of DW.

2.6. Evaluation of antioxidant activities

2.6.1. DPPH radical scavenging activity

DPPH radical scavenging assay was carried out as described by Rufino et al.[35] to determine antioxidant activity of PvAE and AgNPs. The reaction mixture consisted of ethanol, acetate buffer (pH 5.5, 100 mM), 500 μM DPPH (diluted in ethanol), and sample (PvAE (0.3 or 30 mg mL^{-1}) or $AgNO_3$ (5 mM) or AgNPs). After 30 min in dark, absorbance was read at 517 nm with an UV–vis spectrophotometer (Bel Photonics, Brazil) and results were determined as percentage of antioxidant activity compared to control (solution without samples).

2.6.2. Ferric ion reducing antioxidant power (FRAP)

FRAP assay followed protocol of Guimarães et al.[36], in which 90 μL sample (PvAE (0.3 or 30 mg mL^{-1}) or $AgNO_3$ (5 mM) or AgNPs), 270 μL ultrapure water and 2.7 mL FRAP reagent were mixed and incubated at 37 °C for 30 min. After reaching room temperature, absorbance was read at 593 nm with an UV–Vis spectrophotometer (Bel Photonics, Brazil) and results were determined as μM Trolox equivalent (TE) per gram of sample.

2.6.3. Inhibition of lipid peroxidation (TBARS)

TBARS assay was performed following method of Raharjo et al.[37], using egg yolk homogenate as the substrate. This substrate was mixed with sample (PvAE (0.3 or 30 mg mL^{-1}) or $AgNO_3$ (5 mM) or AgNPs) and 2,2′-Azobis(2-methylpropionamidine) dihydrochloride (AAPH) (0.12 M). This mixture was heated at 37 °C for 30 min and after cooling it reacted with trichloroacetic acid and thiobarbituric acid. The resulting mixture was heated at 97 °C for 15 min and centrifuged for 10 min at 3,000 rpm. Afterwards, the absorbance of supernatant was read at 532 nm and inhibition of lipid peroxidation was determined as percentage compared to control (solution without sample). Trolox (0.14 mg mL^{-1}) is used as positive control.

2.6.4. Oxygen radical absorbance capacity (ORAC)

ORAC assay was conducted according to Dávalos et al.[38]. 130 μL Fluorescein (100 nM) was used as fluorescent probe and it was mixed with 20 μL of sample (PvAE (0.3 or 30 mg mL^{-1}) or AgNPs) and 50 μL AAPH in a microplate for fluorescence analysis. Fluorescence decay was measured every 5 min for 2 h at 37 °C with a fluorometer adapted for microplates (Synergy H1 Hybrid Reader, Biotek) at 470 nm excitation and 520 nm emission. ORAC values were calculated by the comparison between areas under the fluorescence of samples and blank.

2.6.5. Oxidative hemolysis test

Oxidative hemolysis assay described by Yang et al.[39] and Khare et al.[40] was used to determine antioxidant activity. A 10 % erythrocyte suspension was incubated with AAPH (50 mM) and samples (PvAE (0.3 or 30 mg mL^{-1}) or AgNPs) at 37 °C for 6 h. Hemolysis was monitored hourly by centrifugation of aliquots of solution and measurement of supernatant at 540 nm. Hemolysis percentage was calculated as percentage compared to positive (erythrocyte suspension with AAPH) and negative (erythrocyte diluted in phosphate-buffered saline (PBS)) controls.

2.7. Evaluation of antiglycation activity of PvAE and AgNPs

2.7.1. Preparation of glycation reaction mixture

Glycation reaction mixtures were prepared for the antiglycation evaluation using bovine serum albumin (BSA) (2 mg mL^{-1}) (Sigma-Aldrich, Brazil) diluted in PBS (pH 8; 10 mM) with ribose (1 M) (Sigma-Aldrich, Brazil). Treatments were prepared in the presence or absence of aminoguanidine (AMG, 40 mM) or sample (PvAE (0.3 or 30 mg mL^{-1}) or AgNPs) and were incubated at 37 °C for 7 days to determine free amino groups and relative eletrophoretic mobility (REM) or 15 days to determine inhibition of AGEs formation.

2.7.2. Determination of free amino groups

The method described by Fayle et al.[41] was used to determine free amino groups in the glycation reaction mixture. Ortho-phthaldialdehyde (OPA) (Sigma-Aldrich, Brazil) was used to prepare OPA reagent by mixing 25 mL sodium borate (0.1 M), 2.5 mL sodium dodecyl sulfate (SDS, 20 %), 100 μL 2-mercaptoethanol (Sigma-Aldrich, Brazil), and 40 mg OPA (dissolved in 1 mL methanol). Sample (glycation reaction mixture) was mixed with OPA reagent and then reacted for 2 min at room temperature. Absorbance was read at 340 nm, and results were expressed as percentage of free amino groups compared to glycation mixture with only BSA.

2.7.3. Inhibition of advanced glycation end-products (AGEs) formation

Inhibition of AGEs formation was conducted according to Rahbar and Figarola.[42] Sample (glycation reaction mixture) was mixed with OPA reagent (prepared as described above) and reacted at 37 °C for 2 min. AGEs formation was determined by the evaluation of fluorescent characteristics using a spectrofluorometer at 360 nm (excitation) and 460 nm (emission). Values of AGEs inhibition were expressed as percentage compared to control.

2.7.4. Relative electrophoretic mobility (REM)

For determination of antiglycation potential by REM assay was used method describe by Perera and Handuwalage.[43] Sodium dodecyl sulfate–polyacrylamide gel electrophoresis (SDS-PAGE) was performed using 4 % stacking gel and 12 % separation gel. Glycation reaction mixtures were heated at 95 °C for 10 min and applied to the gel. The electrophoresis process was conducted for approximately 3 h and bands were visualized after staining with Coomassie-Blue (R-250) (Sigma-Aldrich, Brazil). Appearance and intensity of bands were compared between samples and controls to determine antiglycation activity.

2.8. Evaluation of anti-aging activity

2.8.1. Inhibitory activity on collagenase, elastase and tyrosinase

2.8.1.1. Collagenase inhibitory activity. Collagenase inhibitory activity was evaluated using EnzCheck® Gelatinase/Collagenase Kit (Molecular Probes Eugen OR). PvAE was analyzed at concentrations of 10, 50, and 100 μg mL^{-1}. Treatments were performed in 96-well fluorescence microplates, which were submitted to kinetic reading in a spectrofluorometer at 495 nm (excitation) and 515 nm (emission) at 37 °C for 35 min.

2.8.1.2. Elastase inhibitory activity. Elastase inhibitory activity was determined using the EnzCheck® Elastase Kit (Molecular Probes). PvAE was analyzed at concentrations of 10, 50, and 100 μg mL^{-1}. Treatments were performed in 96-well fluorescence microplates, which were

submitted to kinetic reading in a spectrofluorometer at 505 (excitation) and 515 nm (emission) at 37 °C for 35 min.

2.8.1.3. Tyrosinase inhibitory activity. Tyrosinase inhibitory activity was analyzed as described by Khatib[44] using a UV–Vis spectrophotometer (Bel Photonics, Brazil). Phosphate buffer, tyrosinase, and PvAE (10, 50, or 100 μg mL^{-1}) or kojic acid (70 μg mL^{-1}) were mixed. Afterwards, L-tyrosine solution was added to the mixture, which was incubated for 20 min. Absorbance was measured at 475 nm and results were expressed as percentage compared to control.

2.8.2. Molecular docking analysis

The major compounds from PvAE (β-sitosterol, Hexadecanoic acid, Meso-inositol, N-Hentriacontane, 9-Octadecenoic acid (Z)-methyl ester and Propanoic acid) were subjected for molecular docking. Enzyme-ligand docking was conducted for type IV collagenase (PDBid: 1QIB), elastase (PDBid: 1ELE), and tyrosinase (PDBid: 5M8P) using GOLD v.2020, while DNA-ligand interactions were conducted with DNA molecule (PDBid: 2ROU) using AutoDock Vina v.1.2.0.[45] Binding interactions were analyzed using CHIMERA 1.8 (ref. 46) and BIOVIA (Dassault Systèmes, Discovery Studio Visualizer, version 20, San Diego: Dassault Systèmes, 2019), which were selected to generate 3D and 2D visualization of interactions.

2.9. Statistical analysis

All results were expressed as mean ± standard deviation. OriginLab Pro® 2018 software was used for statistical analysis. Comparisons between treatments were made using one-way ANOVA, followed by Tukey's post-hoc test, with significance set at $p \leq 0.05$.

3. Results and discussion

3.1. HPLC analysis of PvAE

HPLC demonstrated the presence of phytoconstituents such as β-sitosterol, Meso-inositol, N-Hentriacontane, Hexadecanoic acid, 9-Octadecenoic acid (Z)-methyl ester, 9,12-Octadecadienoic acid methyl ester and Propanoic acid in *P. venusta* extract (Table 1 and Fig. 1). These constituents were also observed by Roy et al.,[47] Figueiredo et al.,[48] and Kusmardiyani et al.[13] that reported that the antioxidant activity might be associated with the compounds identified in PvAE.

The AgNPs formation through green synthesis promoted by the mixture of PvAE and $AgNO_3$ was demonstrated by the color change from yellow brown to dark brown (Fig. 2). Efficiency of synthesis was directly associated with parameters and conditions including $AgNO_3$ and PvAE concentrations, pH and temperature/time influenced on the extinction spectra of AgNPs as shown in Fig. 3. The best parameters and conditions for AgNPs formation were defined as 5 mM $AgNO_3$, 0.3 mg mL^{-1} PvAE, pH 10 at 30 °C for 60 min, which demonstrated peaks around 400–420 nm (Fig. 4).

The green synthesis of AgNPs using PvAE presented similar results

Table 1
Phytoconstituents identified in *Pyrostegia venusta* extract by HPLC.

RT	Name of Compound	Chemical formula	Molecular weight (MW)	Peak Area (%)
5.478	β-sitosterol	$C_{29}H_{50}O$	414.71	4.952
6.432	Meso-inositol	$C_6H_{12}O_6$	180.161	5.836
12.695	N-Hentriacontane	$C_{31}H_{64}$	436.851	16.358
23.473	Hexadecanoic acid	$C_{17}H_{34}O_2$	274.20	9.645
26.878	9-Octadecenoic acid (Z)-methyl ester	$C_{19}H_{36}O_2$	296.50	4.124
27.872	9,12-Octadecadienoic acid methyl ester	$C_{19}H_{34}O_2$	294.50	6.231
36.402	Propanoic acid	$C_3H_6O_2$	74.08	11.458

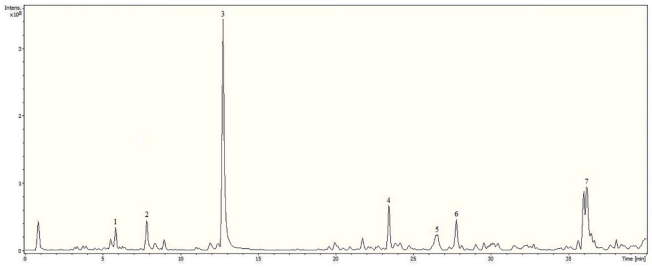

Fig. 1. Chromatograms of *P. venusta* extract obtained by High Performance Liquid Chromatography (HPLC) highlighting the presence of β-sitosterol (1), Meso-inositol (2), N-Hentriacontane (3), Hexadecanoic acid (4), 9-Octadecenoic acid (Z)-methyl ester (5), 9,12-Octadecadienoic acid methyl ester (6) and Propanoic acid (7).

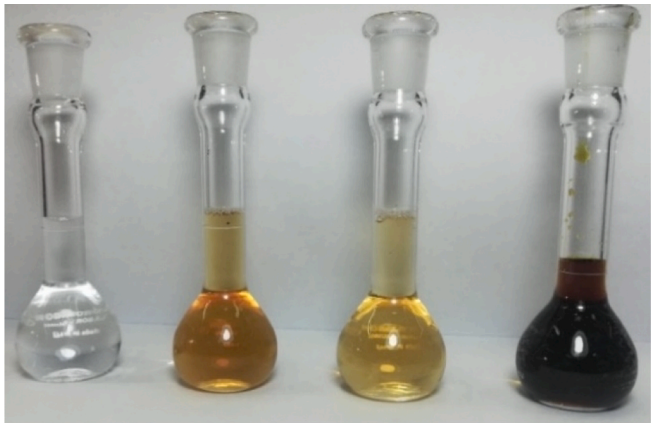

Fig. 2. Change in color of solutions containing: (A) silver nitrate ($AgNO_3$); (B) *Pyrostegia venusta* aqueous extract (PvAE); (C) $AgNO_3$ and PvAE (D) silver nanoparticles (AgNPs) exhibiting a dark brown color that indicates AgNPs formation.

than those observed by Bhat et al.[49] obtained a dark brown solution after the synthesis process and exhibited a characteristic extinction spectrum for colloidal AgNPs dispersions with peaks varying from 370 to 420 nm.

3.2. AgNPs characterization

Fig. 5A presents Scanning Transmission Electron Microscopy (STEM) image of the colloidal solution containing AgNPs synthesized using PvAE, which shows NPs of different sizes (varying from 19 nm to 22 nm). Fig. 5B shows that AgNPs presented a mean size of 20.24 nm and a zeta potential of −21.94 mV, which may indicate stability of the AgNPs colloidal solution. In addition, it exhibited a polydispersity index (PDI) of 0.6094 Molecular weight/Average molecular weight (Mw/Mn) that was also presented in Table 2. This PDI value may suggest a variable size of AgNPs and different forms of aggregation within the colloidal solution. Furthermore, two main peas were identified in DLS analyses, where Peak 1 represents 74.01 % of the readings and exhibited average intensity of 61.22 nm, while Peak 2 represents 24.22 % of the readings and exhibited average intensity of 5.925 nm.

DLS analyses of the AgNPs presented spherical and polydisperse NPs and exhibited low agglomeration between them. The mean size values (20.24 nm) observed corroborate with those exhibited in STEM. This result is similar to previous results observed by Bhat et al.[49] that reported the formation of AgNPs through green synthesis using *P. venusta* leaf extract Zanco et al.[50] also demonstrated that *P. venusta* leaves ethanolic extract can be used to produce nanostructures (liposomes and

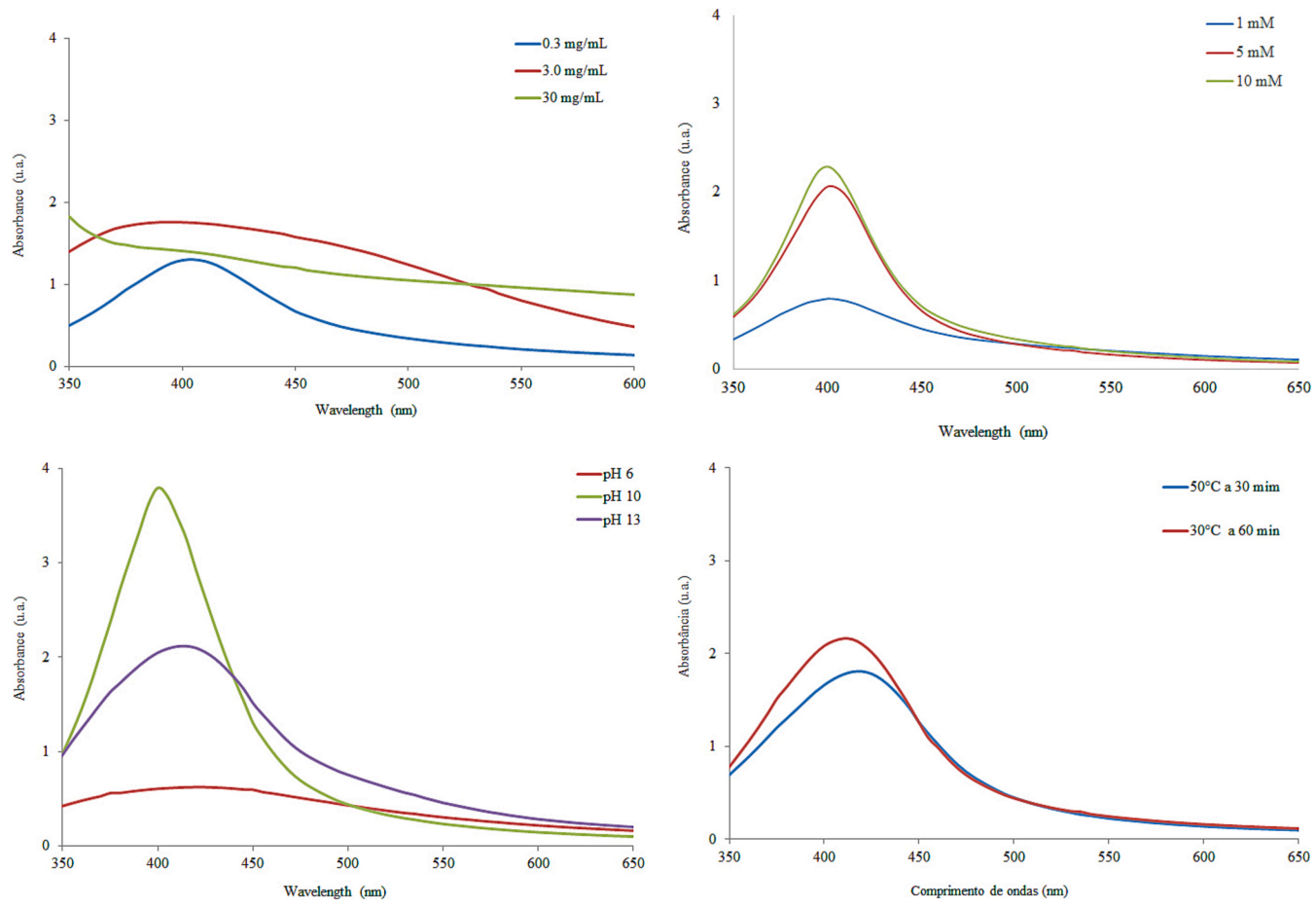

Fig. 3. Extinction spectra of silver nanoparticles (AgNPs) formed by varying parameters, where A: *Pyrostegia venusta* aqueous extract (PvAE) concentration, B: silver nitrate ($AgNO_3$) concentration, C: pH, D: temperature/time.

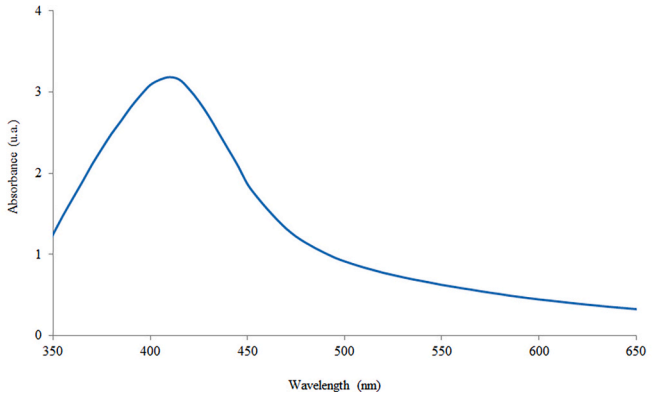

Fig. 4. Extinction spectra of silver nanoparticles (AgNPs) formed under the best parameters: 5 mM silver nitrate ($AgNO_3$), 0.3 mg mL^{-1} Pyrostegia venusta aqueous extract (PvAE), pH 10, and 60 min at 30 °C.

polymeric nanoparticles). Thus, this study demonstrates that flower extracts from *P. venusta* are also able to reduce metal salts to produce nanostructured products with nanobiotechnological application.

Fig. 6 displays the FTIR spectra of PvAE and AgNPs, where several vibrational bands associated with organic functional groups can be identified. Notably, rounded bands appear in the ranges of 3373–3226 cm^{-1}, 2947–2874 cm^{-1}, 1401–1323 cm^{-1}, and 1153–1125 cm^{-1}, corresponding to the stretching vibrations of alcoholic (O–H), alkane (C–H), phenolic, and carbonyl (C–O) groups, respectively. Additionally, the presence of a band between 1540–1520 cm^{-1} may be attributed to the stretching mode of carbonyl group (C=O), which suggests the presence of compounds such as carboxylic acids, aldehydes, esters, or ketones.

FTIR spectra indicates the presence of organic compounds (phytoconstituents) in the nanoparticles, supporting the successful synthesis of AgNPs mediated by bioactive compounds of PvAE. Therefore, FTIR spectra corroborates with UV-vis data, providing evidence of molecular interactions between the synthesized AgNPs and phytoconstituents, which influence the optical properties and particle sizes of AgNPs. These findings are in accordance with results presented by Kambale et al.,[51] who demonstrated that FTIR analysis reveals the bioreductive efficiency of various plant extracts for the synthesis of AgNPs. Furthermore, these spectra support UV–Vis analysis, indicating molecular interactions between the synthesized AgNPs and phytoconstituents, which influenced optical absorption and particle size distribution of the AgNPs as well as reported by Tesfaye et al.[52] Lastly, AgNPs exhibited distinct vibrational FTIR profiles, demonstrating the variety of compounds present on particles surface, which was also observed by Pasieczna-Patkowska et al.[53]

3.3. Phytochemical compounds of PvAE and AgNPs

Table 3 exhibits total polyphenols and flavonoids content of PvAE and AgNPs. PvAE presented the highest total polyphenols (325.78 mg GAE g^{-1} DW) and flavonoids (304.20 mg RE g^{-1} DW) at the greatest concentration (30 mg mL^{-1}). On the other hand, AgNPs presented 132.26 mg GAE g^{-1} DW for total polyphenols and 373.53 mg RE g^{-1} DW for total flavonoids.

Total polyphenols and flavonoids observed in this study corroborate

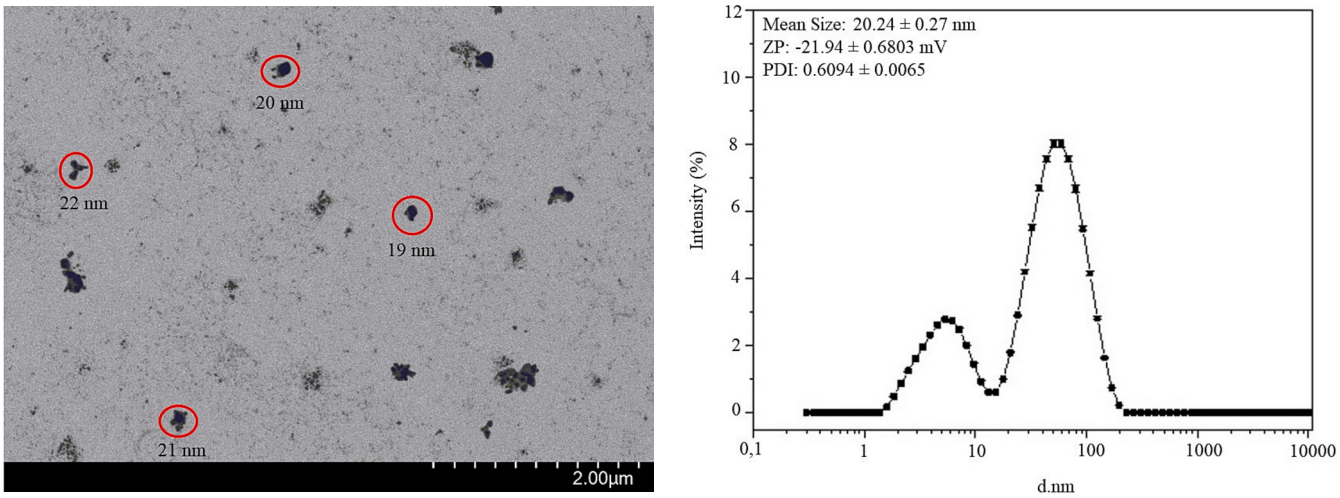

Fig. 5. Scanning transmission electron microscopy (STEM) images of grid-dried silver nanoparticles (AgNPs) formed through green synthesis using *Pyrostegia venusta* aqueous extract (PvAE) (A). Dynamic light scattering (DLS) analysis showing size distribution, zeta potential (ZP), and polydispersity index (PDI) values (B). (For interpretation of the references to color in this figure legend, the reader is referred to the web version of this article.)

Table 2
DLS results of silver nanoparticles (AgNPs) formed through green synthesis using *Pyrostegia venusta* aqueous extract (PvAE).

Analysis	Mean	Standard deviation	RSD	Minimum	Maximum
Size (nm)	20.24	0.272	1.343	19.73	20.72
Polydispersity Index (Mw/Mn)	0.6094	0.006586	1.081	0.6008	0.623
Peak 1 average intensity per area (nm)	61.22	1.503	2.455	59.16	64.07
Peak 1 area per intensity per area (%)	74.01	1.839	2.484	71.93	78.07
Peak 2 average intensity per area (nm)	5.925	0.9648	16.28	3.728	9.084
Peak 2 area per intensity per area (%)	24.22	3.608	14.90	14.41	27.97

Dynamic light scattering (DLS) analysis showing size distribution, zeta potential (ZP), and polydispersity index (PDI) values (B).

with those reported in previous studies conducted by Braga et al.[54], Chaudhary et al.[12] and Darshana and Hemant[55] that evaluated extracts from different *P. venusta* plant parts (leaves, flowers and callus) and observed the presence of several phenolic compounds. AgNPs presented higher flavonoids content, which is similar to results observed by Rani et al.[56] and Velgosová et al.[57] that described an increase in the presence of phytochemical compounds that may be associated with their availability after the process of AgNPs formation.

Table 3
Total polyphenols and flavonoids content of *P. venusta* aqueous extract (PvAE) and AgNPs.

Treatment	Concentration (mg mL^{-1})	Total polyphenols[1]	Total flavonoids[2]
PvAE	0.3	80.78 ± 26.04a	94.87 ± 7.98a
	30	325.78 ± 27.32b	304.20 ± 4.20b
AgNPs	0.3 + 5 mM $AgNO_3$	132.26 ± 29.91c	373.53 ± 28.17c

Results presented as mean ± standard deviation. [1]mg gallic acid equivalent (GAE) g^{-1} dry weight (DW); [2]mg rutin equivalent (RE) g^{-1} DW. Equal letters within the same column indicate no significant differences between samples by Tukey test ($p < 0.05$).

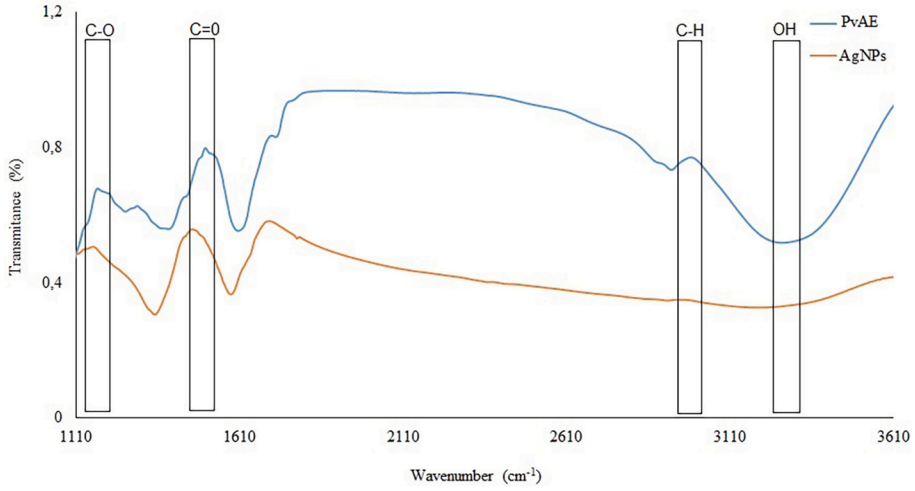

Fig. 6. Fourier transform infrared spectra (FTIR) of *P. venusta* aqueous extract (PvAE) and silver nanoparticles (AgNPs).

3.4. Antioxidant activity of PvAE and AgNPs

Results of *in vitro* antioxidant activity tests are presented in Table 4. PvAE exhibited 74.90 % antioxidant activity at 30 mg mL^{-1} and it differed from all treatments and positive control (Gallic acid) that exhibited 87 % antioxidant activity. In FRAP test, AgNPs exhibited the highest antioxidant activity (862.00 μM TE g^{-1}), which were significant different from both PvAE concentrations. AgNPs also exhibited the highest antioxidant activity among treatments in TBARS test (53.97 % inhibition of TBARS formation), although, this result did not differ from the antioxidant activity at the highest PvAE concentration but differed significantly from positive control (61.80 %).

Fluorescence decay curves of PvAE and AgNPs observed in ORAC assay are presented in Fig. 7. PvAE exhibited antioxidant potential evaluated by fluorescence decay curves through time, although, values were lower than positive control. However, AgNPs presented the greatest antioxidant potential among all treatments and positive control.

The inhibitor effects of PvAE and AgNPs on hemolysis of human erythrocytes induced by AAPH through time are presented in Fig. 8. Both PvAE and AgNPs demonstrated hemolysis inhibitory activity during the period of evaluation, although AgNPs exhibited the highest hemolysis inhibition (85.36 %), which was the greatest at the 6th hour of incubation.

3.5. Antiglycation activity of PvAE and AgNPs

Antiglycation activity of PvAE and AgNPs on BSA exposed to ribose are presented in Fig. 9. Fig. 9A demonstrates the percentage of free amino groups, which was the highest in BSA exposed to ribose and treated with AgNPs (35.41 %), although, it was significantly higher than BSA exposed to ribose and treated with PvAE and lower than positive control (BSA exposed to ribose and treated with AMG). Similarly, BSA exposed to ribose and treated with AgNPs presented the highest inhibition of AGEs formation (85.44 %); however, this value did not differ statistically from BSA exposed to ribose treated with PvAE at 30 mg mL^{-1} (79.23) or positive control (BSA exposed to ribose and treated with AMG) as shown in Fig. 9B.

Electrophoretic profiles of BSA (1), BSA + Ribose (2), BSA + Ribose + AMG (3), BSA + Ribose + PvAE (30.0 mg mL^{-1}) (4), and BSA + Ribose + AgNPs (5) are presented in Fig. 10. Band 2 showed a characteristic protein degradation promoted by BSA exposure to ribose, while Bands 3, 4, and 5 presented an inhibition of this degradation process, which demonstrates antiglycation activity of these samples. The highest antiglycation activity was observed on BSA exposed to ribose and treated with PvAE (Band 4) showing similar intense blue color and wide band from BSA alone (Band 1). On the other hand, BSA exposed to ribose and treated with AgNPs (Band 5) showed antiglycation activity similar to negative control (Band 3), indicating AgNPs exhibits comparable effect to a known antiglycation agent (AMG).

Natural products have been studied for their bioactive compounds and their ability to inhibit glycation, which can suppress inflammatory response, reduce oxidative stress, and consequently work as an effective strategy to delay human aging and prevent the development of different diseases [58]. In this study, PvAE and AgNPs exhibited antiglycation activity in REM assay that may be associated with amino groups that were prevented from reacting with the reducing sugar and inhibition of AGEs formation.

Table 4
Antioxidant activity of *P. venusta* aqueous extract (PvAE), silver nitrate ($AgNO_3$), AgNPs synthesized using PvAE, and positive controls (Gallic acid for DPPH test and Trolox for TBARS test).

Treatment	Concentration (mg mL^{-1})	DPPH[1]	FRAP[2]	TBARS[3]
PvAE	0.3	60.84 ± 0.36a	282.00 ± 1.68a	35.96 ± 7.96a
	30	74.90 ± 0.73b	745.67 ± 16.79b	50.61 ± 3.31b
$AgNO_3$	5 mM	–	–	–
AgNPs	0.3 + 5 mM $AgNO_3$	67.60 ± 0.90c	862.00 ± 29.42c	53.97 ± 5.03b
Gallic acid	0.10	87.00 ± 0.24d	ND	ND
Trolox	0.14	ND	ND	61.80 ± 0.38c

Results presented as mean ± standard deviation. ND: not determined. [1]% Antioxidant activity, [2]μM Trolox equivalent (TE) g^{-1} and [3]% inhibition of TBARS formation. Equal letters within the same column indicate no significant differences between samples by Tukey test ($p < 0.05$).

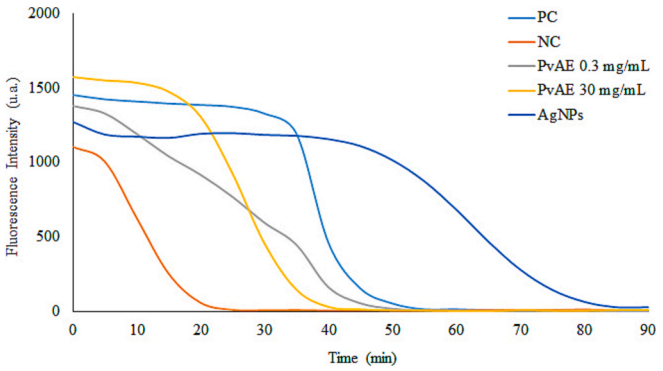

Fig. 7. Fluorescence decay curves obtained by ORAC assay of P. venusta aqueous extract (PvAE) at 0.3 or 30 mg mL^{-1}, silver nanoparticles (AgNPs), negative control (NC) and positive control (PC – Trolox). Fluorescence values were read from 0 to 90 min.

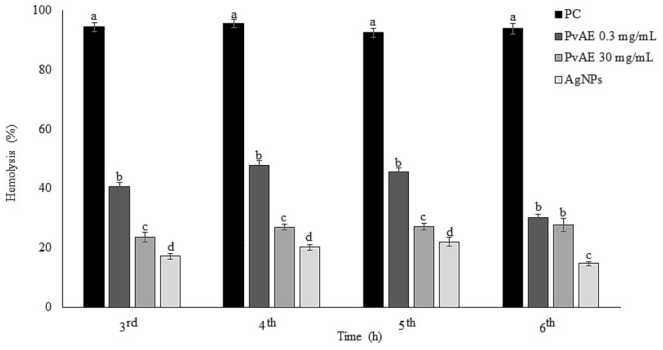

Fig. 8. Inhibitory effects of *Pyrostegia venusta* aqueous extract (PvAE) and silver nanoparticles (AgNPs) on the hemolysis of human erythrocytes induced by AAPH. Treatments were evaluated after 3, 4, 5 and 6 h of incubation and values are expressed as mean ± standard error. Equal letters within the same period indicate no significant differences among samples by Tukey test ($p \leq 0.05$).

3.6. Anti-aging activity of PvAE

3.6.1. Inhibitory activity on collagenase, elastase and tyrosinase

Results of inhibitory activity of PvAE at different concentrations (10, 50 or 100 μg mL^{-1}) on collagenase, elastase, and tyrosinase are presented in Fig. 11. PvAE exhibited inhibitory activity in a concentration-dependent manner and the greatest action was observed at the highest concentration, although results were significantly different from positive control (PC) and other concentrations. PvAE presented 63.14 % collagenase inhibition (Fig. 11A), 78.47 % elastase inhibition (Fig. 11B), and 73.26 % tyrosinase inhibition (Fig. 11C).

Collagen and elastin are extracellular matrix biomolecules that are essential to maintain flexibility, elasticity, and strength of skin. Both biomolecules are rapidly degraded and cleaved during cell ageing due to

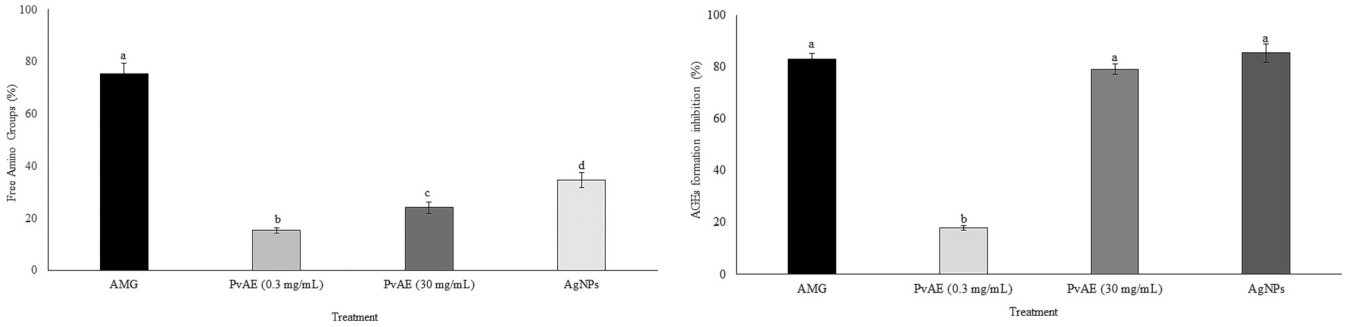

Fig. 9. Antiglycation activity of Aminoguanidine (AMG), Pyrostegia venusta aqueous extract (PvAE) at different concentrations (0.3 or 30 mg mL^{-1}) or silver nanoparticles (AgNPs) on bovine serum albumin (BSA) exposed to ribose (RIB) in the evaluation of free amino groups (A) and inhibition of advanced glycation end-products (AGEs) formation (B). Values followed by equal letters do not show significant difference by Tukey test ($p \leq 0.05$).

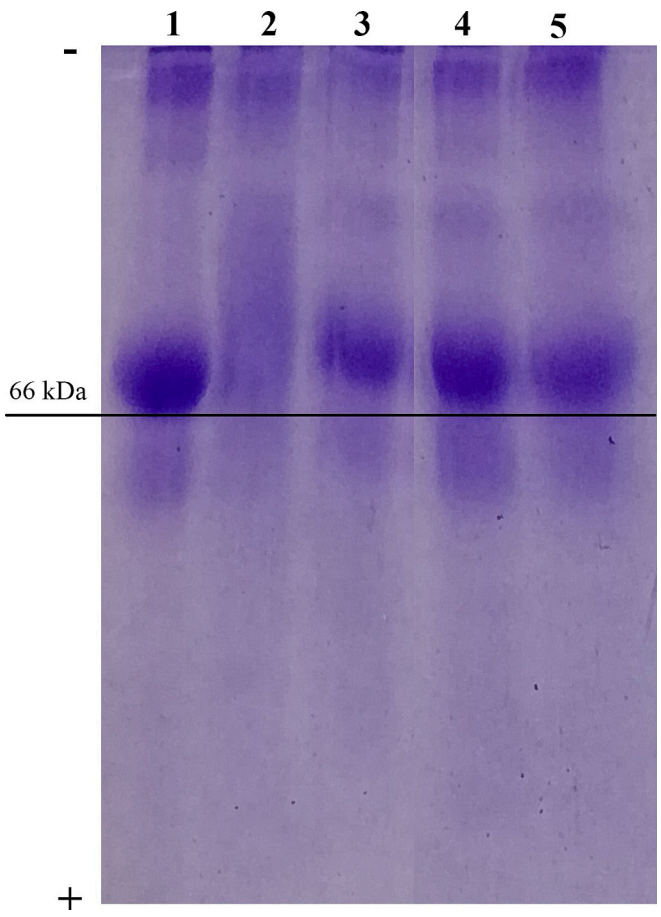

Fig. 10. Antiglycation activity evaluated by Relative electrophoretic mobility (REM), where: 1 = BSA; 2 = BSA + Ribose; 3 = BSA + Ribose + Aminoguanidine (AMG); 4 = BSA + Ribose + Pyrostegia venusta aqueous extract (PvAE) (30 mg mL^{-1}), and 5 = BSA + Ribose + Silver nanoparticles (AgNPs).

overexpression of metalloproteinases such as collagenase and elastase. In addition, these enzymes can stimulate other metalloproteinases leading to an accelerated degradation of various tissue and organs.[59] Considering that, the inhibition of collagenase and elastase promoted by PvAE would be beneficial to avoid premature aging and degradation of biomolecules from the extracellular matrix. On the other hand, melanin is a large group of pigments produced by melanocytes that are derived from tyrosine. Tyrosinase is a copper-containing metalloenzyme that mediates the transformation of tyrosine into 3,4-hihydroxyphenylalanine (DOPA) via hydroxylation, which is oxidized to produce DOPA quinone, a melanin precursor. Overproduction of melanin results in hyperpigmentation and is strongly related to aging and cellular senescence.[52] In the present study, it is possible to observe the inhibition of tyrosinase promoted by PvAE and this activity may be associated with a reduction in damage caused by hyperpigmentation. Similar studies carried out by Abdelfattah et al.,[59] Figueiredo et al.[48] and Bras et al.[60] showed that plant extracts and their active compounds have inhibitory activity on enzymes correlated with premature ageing, including collagenase, elastase, and tyrosinase.

3.6.2. *Molecular docking analysis*

Enzyme-ligand docking was performed using β-sitosterol, Meso-inositol, N-Hentriacontane, Hexadecanoic acid, 9-Octadecenoic acid (Z)-methyl ester or Propanoic acid to identify their potential to bind collagenase, elastase or tyrosinase (Table 5). Best score hits were selected for each ligand, in which N-Hentriacontane exhibited the best docking scores for Collagenase (94.8267), Elastase (79.3796) and Tyrosinase (90.3285).

3D and 2D visualizations of interactions between ligand with best score (N-Hentriacontane) and enzymes (Collagenase, Elastase or Tyrosinase) are shown in Fig. 11. N-Hentriacontane presented bonds with residues Tyr155, Phe168, His166, Ala165, Leu163, His201, Pro221, Val 198, Glu202, Tyr223, Leu218, Phe232, Thr 229, Arg233, and Asn 231 from Collagenase (Fig. 12A). It exhibited bonds with residues Gln155, Leu156, Asn153, Leu149, Trp179, Phe223, Gln200, Val224, Ser225, Thr182, Arg226, and Leu227 from Elastase (Fig. 12B). N-Hentriacontane demonstrated bonds with residues Asn318, Arg321, Ala320, Thr391, Gln390, His392, Tyr348, Val196, Gly209, Gln78, Val211, Pro431, Ile432, Glu216, His215, Tyr79, Asp212, and Glu210 from Tyrosinase (Fig. 12C). Similarly, 3D and 2D visualizations of the interaction between ligand with best score (β-sitosterol) and DNA are shown in Fig. 13. β −Sitosterol exhibited two hydrophobic interactions of the Pi-Alkyl type demonstrated by doted magenta lines.

According to Peluso and Chankvetadze,[61] molecular docking is considered a technique to investigate interactions between ligands and target molecules. Molecular docking analysis of the phytoconstituents of PvAE predicted that these compounds interacted with enzymes or DNA. Abdelfattah et al.[59] demonstrated similar results observing interactions between different flavonoids from *Warburgia salutaris* and elastase, collagenase or tyrosinase, and correlating these interactions with enzyme inhibitory activity evaluated by molecular modeling. Studies performed by Figueiredo et al.[48] and Bras et al.[60] also demonstrated a correlation between the predicted interaction between phytoconstituents and enzymes and the enzyme inhibitory activity of these compounds, which corroborates with the findings of the present study.

Molecular docking has been used to elucidate binding properties of flavonoids and DNA molecules as reported in studies carried out by Mudi et al.[62]. The structure-affinity relationship is the interdependency between ligand structures and DNA binding affinity (i.e. DNA-ligand fit), which represents the energy required in the binding process. The

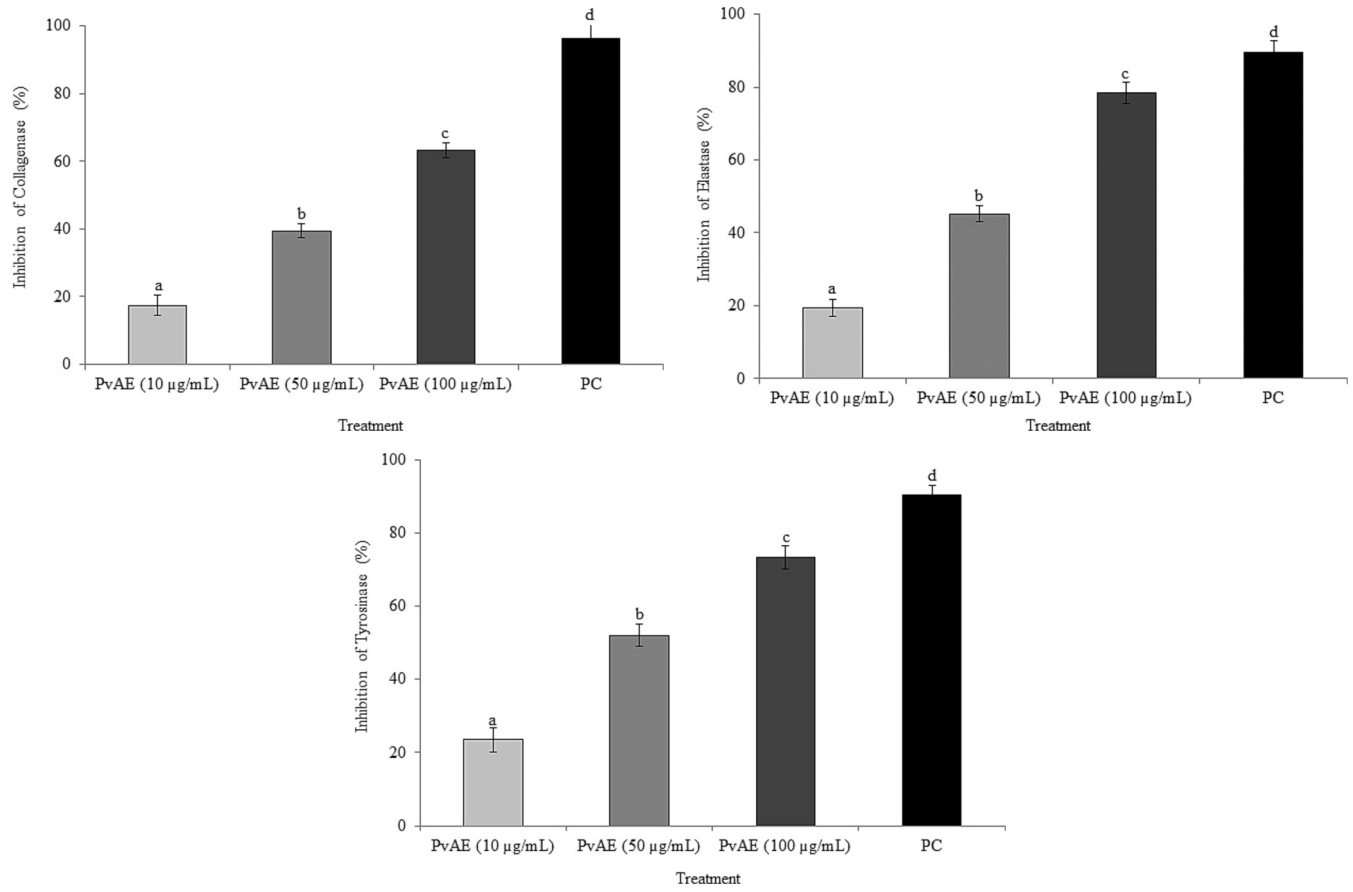

Fig. 11. Inhibitory activity of Pyrostegia venusta aqueous extract (PvAE) at different concentrations (10, 50 or 100 µg mL^{-1}) and positive control (PC) on Collagenase (A), Elastase (B) and Tyrosinase (C).

Table 5
Best score hits for each ligand to enzymes (Collagenase, Elastase, Tyrosinase) and DNA.

Ligands	CHEMPLP			Affinity (kcal/mol) DNA
	Collagenase	Elastase	Tyrosinase	
β −sitosterol	68.5018	61.1462	50.0249	−6.3[a]
Meso-inositol	47.8628	33.8440	59.5883	−5.0
N-Hentriacontane	94.8267[a]	79.3796[a]	90.3285[a]	−5.2
Hexadecanoic acid	74.5206	63.3311	73.2994	−3.2
9-Octadecenoic acid (Z)-methyl ester	77.3199	67.1442	70.0797	−2.8
Propanoic acid	26.6214	26.1646	40.3164	−3.3

[a] Best scores.

molecular docking analyses conducted in the present study made it possible to verify the highest DNA binding affinity. These results indicate the potential of PvAE to interact and act in both pre- and post-transcriptional regulations.

The present study highlights the importance of investigating PvAE and the application of green synthesis method to obtain AgNPs from the bioreduction of silver promoted by active compounds, mainly phenolic compounds, extracted from *P. venusta*. Antioxidant, antiglycation and anti-ageing activities of both the PvAE and AgNPs were evaluated in addition to the *in vitro* anti-aging and in silico evaluations. Thus, results represent an important indicator for the development and discovery of new pharmaceutical and cosmetic formulations based on natural products. Besides, this study demonstrated the possibilities of the application of computational approaches, which would provide information regarding the potential of PvAE compounds for the treatment and prevention of diseases associated with aging and oxidative stress. Therefore, these data stimulate new studies about *P. venusta* focused on the value of this species for pharmacological, cosmetical and nutritional purposes, guaranteeing environmental and cultural benefits.

4. Conclusion

The data obtained in the present study suggests that *P. venusta* aqueous extract (PvAE) acts in the bioreduction and stabilization of silver ions for the green synthesis of silver nanoparticles (AgNPs). In addition, both PvAE and AgNPs showed protective properties against oxidative stress and protein glycation, and inhibited the activity of different enzymes (collagenase, elastase and tyrosinase). These results indicate that the main phenolic compounds found in *P. venusta* (β-sitosterol, Meso-inositol, N-Hentriacontane, Hexadecanoic acid, 9-Octadecenoic acid, (Z)-Methyl ester and Propanoic acid) may be responsible for these activities. Molecular docking analyses showed the predicted interactions between phytoconstituents of *P. venusta* and enzymes, or DNA and these data demonstrated compatibility with experimental data. The present study highlights *P. venusta* and suggests that further studies are needed to analyze the extracts by different methods and evaluate possible applications of these AgNPs in food, pharmaceutical and cosmetic industries.

CRediT authorship contribution statement

Regildo Márcio Gonçalves da Silva: Writing – review & editing. **Pedro Augusto Pereira Rosatto:** Visualization, Methodology, Investigation, Formal analysis, Conceptualization. **Isabelly do Nascimento Pereira:** Visualization, Methodology, Formal analysis,

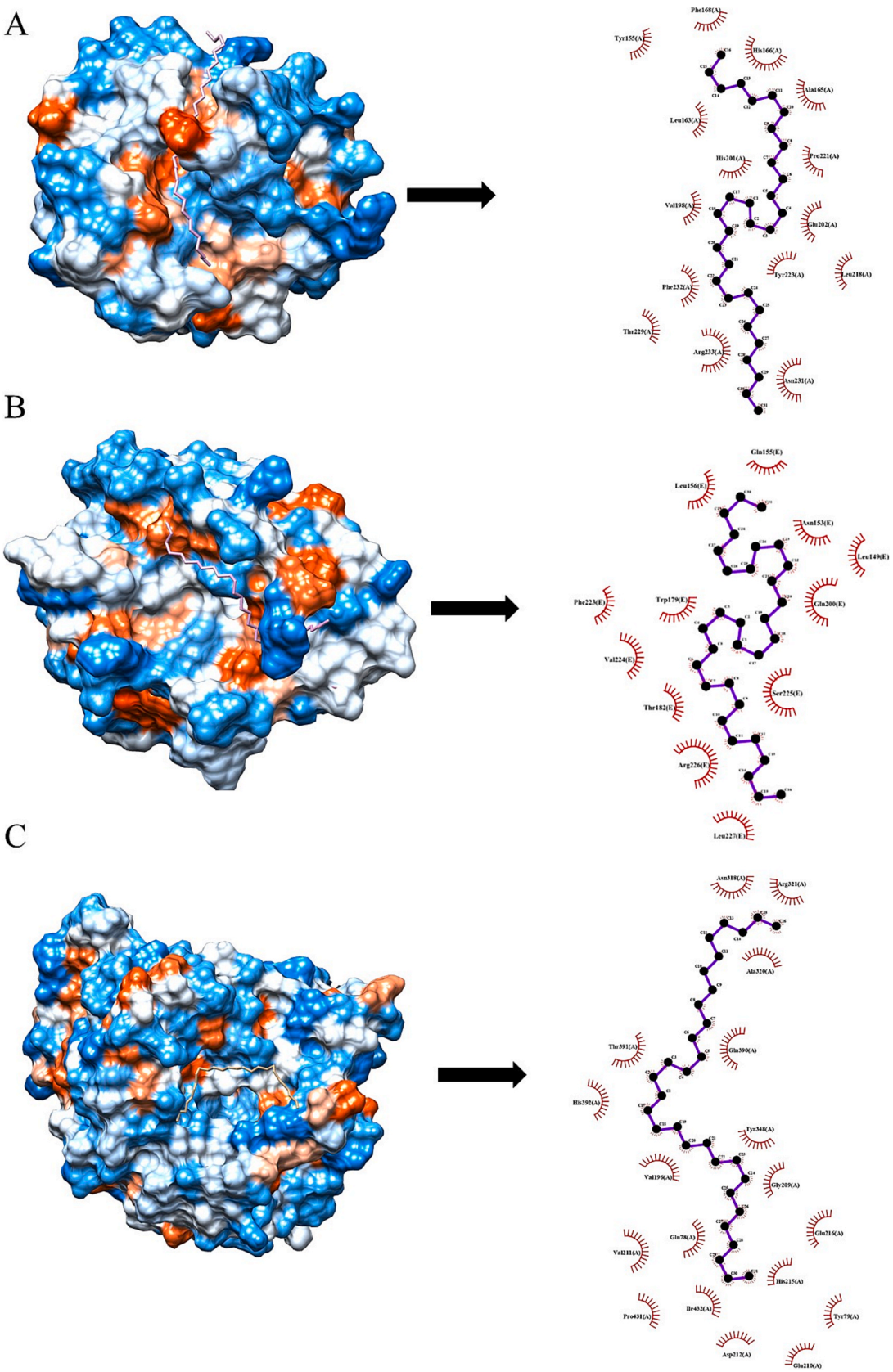

Fig. 12. 3D and 2D visualization of interactions between ligand and enzymes. A: N-Hentriacontane and Collagenase; B: N-Hentriacontane and Elastase; C: N-Hentriacontane and Tyrosinase. 3D molecular targets are presented in hydrophobic surface visualization and 2D analyses show the main atom interactions between N-Hentriacontane and enzymes.

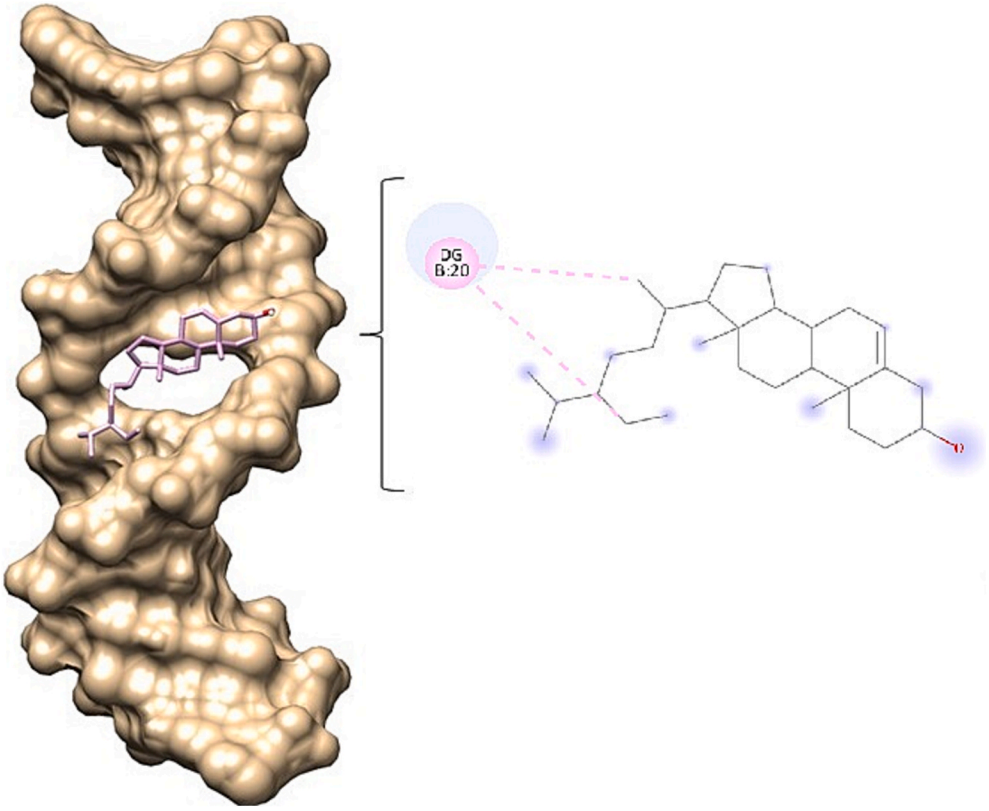

Fig. 13. 3D and 2D visualizations of interaction between ligand (β–sitosterol) and DNA. 3D molecular targets are presented in hydrophobic surface visualization and 2D analysis shows the main atom interactions between ligand and DNA, in which doted magenta lines represent hydrophobic interactions of the Pi-Alkyl type. (For interpretation of the references to color in this figure legend, the reader is referred to the web version of this article.)

Conceptualization. **Laura Camargo Zibordi:** Validation, Methodology, Investigation, Formal analysis, Conceptualization. **Hugo Henrique Santos:** Supervision, Methodology, Investigation, Formal analysis, Conceptualization. **Filipe Oliveira Granero:** Writing – review & editing, Validation, Supervision, Investigation, Formal analysis, Conceptualization. **Célia Cristina Malaguti Figueiredo:** Validation, Supervision, Methodology, Investigation, Formal analysis, Conceptualization. **Patrícia Soares Santiago:** Visualization, Validation, Supervision, Formal analysis, Conceptualization. **Carlos Augusto Prata Gaona:** Visualization, Validation, Supervision, Software, Formal analysis, Conceptualization. **Nilson Nicolau-Junior:** Writing – original draft, Visualization, Supervision, Software, Methodology, Investigation, Formal analysis. **Luciana Pereira Silva:** Visualization, Validation, Supervision, Methodology, Investigation, Formal analysis, Conceptualization.

Declaration of competing interest

The authors declare that they have no known competing financial interests or personal relationships that could have appeared to influence the work reported in this paper.

Acknowledgement

This work was supported by grants 2008/55577-2, 2008/50689-7 and 2009/51209-1, São Paulo Research Foundation (FAPESP).

References

1. Coimbra MC, Chagas RCR, Pádua MS, Vilela MSP, Castro AHF. Growth, morphology, and bioactive phenolic compounds production in *Pyrostegia venusta* calli. *Biocatal Agric Biotechnol.* 2019;18, 101036. https://doi.org/10.1016/j.bcab.2019.101036.
2. Rossato DR, Kolb RM. Comportamento fenológico da liana *Pyrostegia venusta* (Ker Gawl.) Miers (Bignoniaceae) em área de cerradão na Estação Ecológica de Assis, SP, Brasil [Phenological behavior of liana *Pyrostegia venusta* (Ker Gawl.) Miers (Bignoniaceae) in cerrado areas at the Ecological Station of Assis, SP, Brazil]. *Rev Bras Biociênc.* 2011;9(3):289–296.
3. Tunes P, Dötteri S, Guimarães E. Florivory and pollination intersection: changes in floral trait expression do not discourage hummingbird pollination. *Front Plant Sci.* 2022;13, 813418. https://doi.org/10.3389/fpls.2022.813418.
4. Pereira AMS, Hernandes C, Pereira SIV, et al. Evaluation of anticandidal and antioxidant activities of phenolic compounds from *Pyrostegia venusta* (Ker Gawl.). *Miers Chem Biol Interact.* 2014;224:136–141. https://doi.org/10.1016/j.cbi.2014.10.023.
5. Veloso CC, Oliveira MC, Oliveira CC, et al. Hydroethanolic extract of *Pyrostegia venusta* (Ker Gawl.) Miers flowers improve inflammatory and metabolic dysfunction induced by high-refined carbohydrate diet. *J Ethnopharmacol.* 2014;151(1): 722–728. https://doi.org/10.1016/j.jep.2013.11.046.
6. Moreira CG, Carrenho LZB, Pawloski PL, Soley BS, Cabrini DA, Otuki MF. Preclinical evidence of *Pyrostegia venusta* in the treatment of vitiligo. *J Ethnopharmacol.* 2015;68:315–325. https://doi.org/10.1016/j.jep.2015.03.080.
7. Mostafa NM, El-Dahshan O, Singab ANB. Pyrostegia venusta (Ker Gawl.) Miers: a botanical, pharmacological and phytochemical. *Review.* 2013;2:123. http://doi:10.4172/2167-0412.1000123.
8. Iswe DG, Swami H. An overview of the medicinal benefits of *Pyrostegia Venusta. Int J Creat Res Thoughts.* 2021;9(12):e823–e829.
9. Figueiredo CR, Matsuo AL, Pereira FV, et al. *Pyrostegia venusta* heptane extract containing saturated aliphatic hydrocarbons induces apoptosis on B16F10-Nex2 melanoma cells and displays antitumor activity *in vivo*. *Pharmacogn Mag.* 2014;10 (2):S363–S376. https://doi.org/10.4103/0973-1296.133284.
10. Niu C, Aisa HÁ. Upregulation of melanogenesis and tyrosinase activity: potential agents for vitiligo. *Molecules.* 2017;22(8):1303. https://doi.org/10.3390/molecules22081303.
11. Kumar A, Asthana M, Roy P, Amdekar S, Singh V. Phytochemistry and pharmacology of *Pyrostegia venusta*: a plant of Family Bignoniaceae. *Int J Phytomed.* 2013;5(3):257–261.
12. Chaudhary RS, Jain AK, Chatap VK. Comparative phytochemical investigation and determination of flavonoids, alkaloid and antioxidant activity of leaves, stem and flower extract of *Pyrostegia Venusta*. *J Adv Sci Res.* 2020;11(3):197–201.
13. Kusmardiyani S, Noviyanti G, Hartati R, Fidrianny I. *Pyrostegia* genus: an updated review of phytochemical compounds and pharmacological activities. *Biointerface Res App Chem.* 2021;11(3):10664–10678. https://doi.org/10.33263/BRIAC113.1066410678.
14. Antunes Filho S, Santos MS, Santos OAL, et al. Biosynthesis of nanoparticles using plant extracts and essential oils. *Molecules.* 2023;28(7):3060. https://doi.org/10.3390/molecules28073060.

15. Jadoun S, Arif R, Jangib NK, Meena RK. Green synthesis of nanoparticles using plant extracts: a review. *Environ Chem Lett*. 2020;19:355–374. https://doi.org/10.1007/s10311-020-01074-x.
16. Vanlalveni C, Lallianrawna S, Biswas A, Selvaraj M, Changmai B, Rokhum SL. Green synthesis of silver nanoparticles using plant extracts and their antimicrobial activities: a review of recent literature. *RSC Adv*. 2021;11:2804–2837. https://doi.org/10.1039/D0RA09941D.
17. Adrianto N, Panre AM, Istiqomah NI, Riswan M, Apriliani F, Suharyadi E. Localized surface plasmon resonance properties of green synthesized silver nanoparticles. *Nano-Struct Nano-Objects*. 2022;31, 100895. https://doi.org/10.1016/j.nanoso.2022.100895.
18. Azad A, Zafar H, Raza F, Sulaiman M. Factors influencing the green synthesis of metallic nanoparticles using plant extracts: a comprehensive review. *Pharm Fronts*. 2023;5(3):e117–e131. https://doi.org/10.1055/s-0043-1774289.
19. Shashiraj KN, Hugar A, Kumar RS, et al. Exploring the antimicrobial, anticancer, and apoptosis inducing ability of biofabricated silver nanoparticles using *Lagerstroemia speciosa* flower buds against the human osteosarcoma (mg-63) cell line via flow cytometry. *Bioengineering*. 2023;10(7):821. https://doi.org/10.3390/bioengineering10070821.
20. Math HH, Shashiraj KN, Kumar RS, et al. Investigation of *in vitro* anticancer and apoptotic potential of biofabricated silver nanoparticles from *Cardamine hirsuta* (L.) leaf extract against caco-2 cell line. *Inorganics*. 2023;11(8):322. https://doi.org/10.3390/inorganics11080322.
21. Meher A, Tandi A, Moharana S, et al. Silver nanoparticle for biomedical applications: a review. *Hybrid Adv*. 2024;6, 100184. https://doi.org/10.1016/j.hybadv.2024.100184.
22. Zhang N, Sun J, Yin L, Liu J, Chen C. Silver nanoparticles: from *in vitro* green synthesis to *in vivo* biological effects in plants. *Adv Agrochem*. 2023;2(4):313–323. https://doi.org/10.1016/j.aac.2023.08.004.
23. Ijaz I, Bukhari A, Gilani E, et al. Green synthesis of silver nanoparticles using different plants parts and biological organisms, characterization, and antibacterial activity. *Environ Nanotechnol Monit Manage*. 2022;18, 100704. https://doi.org/10.1016/j.enmm.2022.100704.
24. Rudrappa M, Rudayni HÁ, Assiri RA, et al. *Plumeria alba*-mediated green synthesis of silver nanoparticles exhibits antimicrobial effect and anti-oncogenic activity against glioblastoma U118 MG cancer cell line. *Nanomaterials*. 2022;12(3):493. https://doi.org/10.3390/nano12030493.
25. Dhaka A, Mali SC, Sharma S, Trivedi R. A review on biological synthesis of silver nanoparticles and their potential applications. *Results Chem*. 2023;6, 101108. https://doi.org/10.1016/j.rechem.2023.101108.
26. Noori A, Hasanuzzaman M, Roychowdhury R, et al. Silver nanoparticles in plant health: physiological response to phytotoxicity and oxidative stress. *Plant Physiol Biochem*. 2024;209, 108538. https://doi.org/10.1016/j.plaphy.2024.108538.
27. Sies H. Oxidative stress: concept and some practical aspects. *Antioxidants*. 2020;9(9):852. https://doi.org/10.3390/antiox9090852.
28. Deng Y, Wang X, Zhang C, Xie P, Huang L. Inhibitory effect of a chinese quince seed peptide on protein glycation: a mechanism study. *J Bioresour Bioprod*. 2023;8(2):187–197. https://doi.org/10.1016/j.jobab.2023.01.008.
29. Ebert T, Tran N, Schurgers L, Stenvinkel P, Shiels PG. Ageing – Oxidative stress. *Ptms and Disease Mol Asp Med*. 2022;86, 101099. https://doi.org/10.1016/j.mam.2022.101099.
30. Wu Z, Qu J, Zhang W, Liu G-H. Stress, epigenetics, and aging: Unraveling the intricate crosstalk. *Mol Cell*. 2023;84(1):P35–P54. https://doi.org/10.1016/j.molcel.2023.10.006.
31. Vankudoth S, Dharavath S, Veera S, et al. Green synthesis, characterization, photoluminescence and biological studies of silver nanoparticles from the leaf extract of *Muntingia calabura*. *Biochem Biophys Res Commun*. 2022;630:143–150. https://doi.org/10.1016/j.bbrc.2022.09.054.
32. Alharbi NS, Alsubhi NS, Felimban AI. Green synthesis of silver nanoparticles using medicinal plants: Characterization and application. *J Radiat Res Appl Sci*. 2022;15:109–124. https://doi.org/10.1016/j.jrras.2022.06.012.
33. Singleton VL, Rossi JA. Colorimetry of total phenolics with phosphomolybdic-phosphotungstic acid reagents. *Am J Enol Vitic*. 1965;16(3):144–158. https://doi.org/10.5344/ajev.1965.16.3.144.
34. Christ B, Mueller KB. Zur serienmäßigen Bestimmung des Gehaltes an Flavonol-Derivaten in Drogen [on the serial determination of the content of flavonol derivatives in drugs]. *Arch Pharm*. 1960;293(12):1033–1042. https://doi.org/10.1002/ardp.19602931202.
35. Rufino MSM, Alves RE, Brito ES, Pérez-Jiménez J, Saura-Calixto F, Mancini-Filho J. Bioactive compounds and antioxidant capacities of 18 non-traditional tropical fruits from Brazil. *Food Chem*. 2010;121(4):996–1002. https://doi.org/10.1016/j.foodchem.2010.01.037.
36. Guimarães AG, Oliveira GF, Melo MS, et al. Bioassay-guided evaluation of antioxidant and antinociceptive activities of carvacrol. *Basic Clin Pharmacol Toxicol*. 2010;107(6):949–957. https://doi.org/10.1111/j.1742-7843.2010.00609.x.
37. Raharjo S, Sofos JN, Schmidt GR. Effect of meat curing agents and phosphates on thiobarbituric acid (TBA) numbers of ground beef determined by the aqueous acid extraction TBA-C_{18} method. *Food Chem*. 1992;47(2):137–143. https://doi.org/10.1016/0308-8146(93)90235-8.
38. Dávalos A, Gómez-Cordovés C, Bartolomé B. Extending applicability of the oxygen radical absorbance capacity (ORAC-fluorescein) assay. *J Agric Food Chem*. 2004;52(1):48–54. https://doi.org/10.1021/jf0305231.
39. Yang HL, Chen SC, Chang NW, et al. Protection from oxidative damage using *Bidens pilosa* extracts in normal human erythrocytes. *Food Chem Toxicol*. 2006;44(9):1513–1521. https://doi.org/10.1016/j.fct.2006.04.006.
40. Khare S, Singh RK, Prakash O. Green synthesis, characterization and biocompatibility evaluation of silver nanoparticles using radish seeds. *Results Chem*. 2022;4, 100447. https://doi.org/10.1016/j.rechem.2022.100447.
41. Fayle SE, Healy JP, Brown PA, Reid EA, Gerrard JA, Ames JM. Novel approaches the analysis of the Maillard reaction of proteins. *Electrophoresis*. 2001;22(8):1518–1525. https://doi.org/10.1002/1522-2683.
42. Rahbar S, Figarola JL. Inhibitors and breakers of advanced glycation end products (AGEs): a review. *Curr Med Chem.: Immunol. Endocr Metab Agents*. 2002;2(2):135–161. https://doi.org/10.2174/1568013023358889.
43. Perera HKI, Handuwalage CS. Analysis of glycation induced protein cross-linking inhibitory effects of some antidiabetic plants and spices. *BMC Compl Alternative Med*. 201;15:175. Doi: 10.1186/s12906-015-0689-1.
44. Khatib S, Nerya O, Musa R, Shmuel M, Tamir S, Vaya J. Chalcones as potent tyrosinase inhibitors: the importance of a 2,4-substituted resorcinol moiety. *Bioorg Med Chem*. 2005;13(2):433–441. https://doi.org/10.1016/j.bmc.2004.10.010.
45. Trott O, Olson AJ. AutoDock Vina: improving the speed and accuracy of docking with a new scoring function, efficient optimization, and multithreading. *J Comput Chem*. 2010;31(2):455–461. https://doi.org/10.1002/jcc.21334.
46. Pettersen E, Goddard TD, Huang CC, et al. UCSF Chimera–a visualization system for exploratory research and analysis. *J Comput Chem*. 2004;25(13):1605–1612. https://doi.org/10.1002/jcc.20084.
47. Roy P, Amdekar S, Kumar A, Singh V. Preliminary study of the antioxidant properties of flowers and roots of *Pyrostegia venusta* (Ker Gawl) Miers. *BMC Complement Altern Med*. 2011;11:69. https://doi.org/10.1186/1472-6882-11-69.
48. Figueiredo CCM, Gomes AC, Zibordi LC, et al. Biosynthesis of silver nanoparticles of *Tribulus terrestris* food supplement and evaluated antioxidant activity and collagenase, elastase and tyrosinase enzyme inhibition: *In vitro* and *in silico* approaches. *Food Bioprod Process*. 2023;138:150–161. https://doi.org/10.1016/j.fbp.2023.01.010.
49. Bhat MP, Kumar RS, Almansour AL, et al. Characterization, antimicrobial activity and anticancer activity of *Pyrostegia venusta* leaf extract-synthesized silver nanoparticles against COS-7 cell line. *Appl Nanosci*. 2023;13:2303–2314. https://doi.org/10.1007/s13204-021-02120-y.
50. Zanco P, Ferrarini SR, Cruz L, et al. Improved antimutagenic effect of *Pyrostegia venusta* (Ker Gawl.) Miers nanostructured extract in liposome and polymeric nanoparticle. *Braz J Pharm Sci*. 2022;58, e20234. https://doi.org/10.1590/s2175-97902022000X2e20234.
51. Kambale EK, Nkanga CI, Mutonkole BI, Bapolisi AM, Tassa DO, Liesse JI, Krause RWM, Memvanga PB. Green synthesis of antimicrobial silver nanoparticles using aqueous leaf extracts from three Congolese plant species (*Brillantaisia patula*, *Crossopteryx febrifuga* and *Senna siamea*). *Heliyon*. 2020;6(8):e04493. Doi: 10.1016/j.heliyon.2020.e04493.
52. Tesfaye M, Gonfa Y, Tadesse G, Temesgen T, Periyasamy S. Green synthesis of silver nanoparticles using *Vernonia amygdalina* plant extract and its antimicrobial activities. *Heliyon*. 2023;9(6), e17356. https://doi.org/10.1016/j.heliyon.2023.e17356.
53. Pasieczna-Patkowska S, Cichy M, Flieger J. Application of Fourier Transform Infrared (FTIR) Spectroscopy in Characterization of Green Synthesized Nanoparticles. *Molecules, Basel*. 202;30(3):684. Doi: 10.3390/molecules30030684.
54. Braga KQ, Coimbra MC, Castro AHF. *In vitro* germination, callus induction and phenolic compounds contents from *Pyrostegia venusta* (Ker Gawl.) Miers. *Acta Sci Biol Sci*. 201;37(2):151-158. Doi: 10.4025/actascibiolsci.v37i2.26067.
55. Darshana IG, Hemant S. Quantitative analysis of phytoconstituents and *in vitro* antioxidant activity of *Pyrostegia venusta* leaves. *J Chem Health Risks*. 2012;14(2):2012–2017.
56. Rani MP, Raghu KG, Nair MS, Padmakumari KP. Isolation and Identification of α-Glucosidase and Protein Glycation Inhibitors from *Stereospermum colais*. *Appl Biochem Biotechnol*. 2014;173:946–9http://doi 10.1007/s12010-014-0898-y.
57. Velgosova O, Dolinská S, Podolská H, Macák L, Cižmárová E. Impact of plant extract phytochemicals on the synthesis of silver nanoparticles. *Materials*. 2024;17(10):2252. https://doi.org/10.3390/ma17102252.
58. Yeh WY, Hsia SM, Lee WH, Wu CH. Polyphenols with antiglycation activity and mechanisms of action: a review of recent findings. *J Food Drug Anal*. 2017;25(1):84–92. https://doi.org/10.1016/j.jfda.2016.10.017.
59. Abdelfattah MAO, Dmirieh M, Bakrim WB, et al. Antioxidant and anti-aging effects of *Warburgia salutaris* bark aqueous extract: evidence from *in silico*, *in vitro* and *in vivo* studies. *J Ethnopharmacol*. 2022;292, 115187. https://doi.org/10.1016/j.jep.2022.115187.
60. Bras BS, Pereira IN, Zibordi LC, et al. Green synthesis of silver nanoparticles using food supplement from *Avena sativa* L., and their antioxidant, antiglycation, and anti-aging activities: *In vitro* and *in silico* studies. *Food Bioprod Process*. 2024;147:175–188. https://doi.org/10.1016/j.fbp.2024.06.013.
61. Peluso P, Chankvetadze B. Recent developments in molecular modeling tools and applications related to pharmaceutical and biomedical research. *J Pharm Biomed Anal*. 2024;238, 115836. https://doi.org/10.1016/j.jpba.2023.115836.
62. Mudi A, Ray S, Bera M, et al. A multi-spectroscopic and molecular docking approach for DNA/protein binding study and cell viability assay of first-time reported pendent azide bearing Cu (II)-quercetin and dicyanamide bearing Zn(II)-quercetin complexes. *Heliyon*. 2023;9(2), e22712. https://doi.org/10.1016/j.heliyon.2023.e22712.